ORIGINAL PAPER

Pinning Force Scaling Analysis of Polycrystalline MgB$_2$

M. R. Koblischka[1,2] · **A. Wiederhold[1]** · **A. Koblischka-Veneva[1,2]** · **C. Chang[3]**

Abstract

Flux pinning force scaling $f = F_p/F_{p,\max}$ vs. $h = H_a/H_{irr}$ was performed on a variety of pure MgB$_2$ samples, including a spark plasma sintered (SPS) one and a series of samples sintered at various reaction temperatures ranging between 775 and 950 °C. The SPS sample exhibits a well-developed scaling at all temperatures, and also the sintered samples prepared at 950 °C; however, the obtained peak positions of the pinning force scalings are distinctly different: The SPS sample reveals dominating pinning at grain boundaries, whereas the dominating pinning for the other one is point-pinning. All other samples studied reveal an apparent non-scaling of the pinning forces. The obtained pinning parameters are discussed in the framework of the Dew–Hughes' pinning force scaling approach.

1 Introduction

The MgB$_2$ superconductors are interesting for various applications as they offer the metallic character which enables a simple processing route and no involved rare earth materials, which reduces the costs involved [1, 2]. The modern cryocooling techniques enable a temperature of 20 K to be reached, which is commonly accepted as the optimum one for applications of MgB$_2$. Besides these advantages, the still limited critical current densities and the presence of flux jumps require further studies on the acting flux pinning mechanism(s) in MgB$_2$ superconductors [3–10].

The pinning force scaling as introduced by Kramer [11] and Dew–Hughes (DH) [12] is an important tool to study the pinning mechanisms acting in a given superconductor sample. This applies not only for the conventional metallic superconductors, where the pioneering work was performed on, but also for the high-T_c counterparts [13–16] as well as MgB$_2$ [16–20] and the iron-based superconductors [21]. The main difference is given by the use of the irreversibility field, H_{irr} instead of the upper critical field, H_{c2} for the scaling, as H_{irr} determines the upper limit of the flux pinning (= irreversible region in the H-T diagram). The flux pinning can be obtained from the scaled pinning force data $f = F_p/F_{p,\max}$ vs. $h = H_a/H_{irr}$ by a fit to the functional dependence given by the following:

$$f = A(h)^p(1-h)^q \quad . \tag{1}$$

The resulting parameters, p and q, determine the dimensionality and the type of the dominating flux pinning, whereas the numerical parameter A in (1) is obtained from the normalization condition $F_p/F_{p,\max} = 1$. The corresponding peak position, h_0, can be calculated as $h_0 = \frac{p}{p+q}$.

In the model of DH, there are six pinning functions $f(h)$ describing the core pinning using (1): (1) $p = 0$, $q = 2$: normal, volume pinning; (2) $p = 1$, $q = 1$: $\Delta\kappa$-pinning, volume pins; (3) $p = 1/2$, $q = 2$: normal, surface pins; (4) $p = 3/2$, $q = 1$: $\Delta\kappa$-pinning, surface pins; (5) $p = 1$, $q = 2$: normal, point pins; and (6) $p = 2$, $q = 1$: $\Delta\kappa$-pinning, point pins. Furthermore, the function (3) is predicted by Kramer [11] for shear-breaking in the case of a set of planar pins. A seventh function describing the magnetic interaction can be disregarded in the present case. Therefore, the parameter p can assume the values 0, 0.5, 1, 1.5, and 2, which describes the dimensionality of the pins, and the parameter q can only

✉ M. R. Koblischka
miko@shibaura-it.ac.jp; m.koblischka@gmail.com

[1] Experimental Physics, Saarland University, P.O.Box 151150, 66041, Saarbrücken, Germany

[2] Present address: Superconducting Materials Laboratory, Department of Materials Science and Engineering, Shibaura Institute of Technology, Tokyo, 135-8548, Japan

[3] Institut Jean Lamour, UMR CNRS-Université de Lorraine, 54506, Vandœuvre-lès-Nancy, France

take the values 1 and 2, describing the type of pinning (i.e., normal conducting or superconducting).

Having this in mind, the analysis of the pinning force scaling provides important information on the flux pinning properties of a given sample, provided that the F_p data exhibit a proper scaling. To obtain information on the flux pinning in MgB$_2$ samples, we therefore investigated a pure SPS-produced MgB$_2$ sample with its high density close to the ideal value, and several members of a series of sintered, polycrystalline MgB$_2$ samples prepared at various reaction temperatures ranging between 775 and 950 °C. As an interesting result, some of the samples exhibit a well-developed scaling, while others do not. The results obtained are discussed in the framework of the DH pinning model.

2 Experimental Procedures

The sample preparation steps for the SPS sample are described in Ref. [22, 23], and the fabrication of the polycrystalline, sintered samples is discussed in Ref. [24]. All samples were pure samples without any additions. The X-ray analysis and electron backscatter diffraction (EBSD) investigations revealed the presence of small amounts of MgO and MgB$_4$ particles in the samples prepared at reaction temperatures above 850 °C. The MgB$_4$ particles in the SPS sample were found to be located to a large extend along the grain boundaries, and not within the MgB$_2$ grains, so these particles cannot provide additional flux pinning [25]. This is important as the goal of this contribution is to study the basic flux pinning properties of MgB$_2$, which would otherwise be overlaid with the strong pinning provided by the secondary particles embedded in the MgB$_2$ matrix. A thorough magnetic characterization of the SPS sample was presented by Jirsa et al. [26]. The superconducting properties of the samples studied are summarized in Table 1 below, presenting the maximum pinning force, $F_{p,\max}$, the current density at 20 K, $j_c(20\,\mathrm{K})$, in self-field condition,

and trapped fields obtained at 20 K on samples with a 20-mm diameter and 5- or 7-mm thickness, respectively. The samples were state-of-the-art for pure samples, which is revealed by trapped field experiments on two stacked SPS samples with a 20-mm diameter (10-mm thickness), where a trapped field of 4.66 T could be recorded at 20 K (6.25 T at 10 K) [27].

For the magnetic measurements, small samples ($2 \times 2 \times 1.5$ mm^3) were cut from the big pellets. The magnetic measurements were performed using a Quantum Design MPMS3 SQUID system with a $\pm$ 7 T applied field, and Quantum Design PPMS systems equipped either with an extraction magnetometer or with VSM option ($\pm$ 7 T and $\pm$ 9 T applied magnetic field). In all cases, the field was applied perpendicular to the sample surface. The field sweep rate was always 0.36 T/min. The temperatures selected for the investigation were between 5 and 35 K in steps of 5 K. From the magnetization data, the critical current densities, j_c, were evaluated using the extended Bean approach for rectangular samples [28]. The irreversibility lines, $H_{\mathrm{irr}}(H, T)$, were determined using a criterion of 100 A/cm^2.

3 Results and Discussion

In all samples, we had problems with flux jumps at the low temperatures, $T = 5$ K and 10 K. Therefore, these measurements were repeated several times to allow a reconstruction of the enveloping curve(s), which were then used for the pinning force calculation.

Figure 1a–c present the pinning force scaling of samples S800 (a), S850 (b), and SPS (c). The final pinning function according to (1) is obtained from a fit to all data and is indicated by a solid, red line. The pinning force scalings of samples S775 and S950 were already shown in Ref. [19], and the scaling behavior of sample S775 is similar to that of sample S800 shown here (a). The main difference between

Table 1 Scaling parameters A, p, q and h_0 for all MgB$_2$ samples studied here

Sample name T_{reaction}(°C)	A	p	q	h_0	$F_{p,\max}$ (10^6 N/m^3)	j_c(20K) (10^3 A/cm^2)	Trapped fields (T)(20K)
S775	2.59	0.43	1.20	0.26	67.8	176	1.5
S800	2.13	0.34	0.96	0.26	68.2	180	1.42
S805	4.31	0.70	1.75	0.29	110	185	1.50
S850	3.05	0.57	1.21	0.33	57.1	128	1.32
S950	4.20	0.66	1.78	0.32	65.6	135	1.25
SPS	5.12	0.83	1.77	0.21	231	300	1.45

The data shown stem from fits to *all* temperatures measured of a given sample. The maximum pinning forces, $F_{p,\max}$, are the data of the maximal measured values, $F_p = j_c \times B$ at $T = 10$ K, and $j_c(20\,\mathrm{K})$ was measured at self-field. The trapped field values were obtained at $T = 20$ K for samples with a 20-mm diameter and 7-mm thickness [24], whereas the sample SPS had only a thickness of 5 mm [23]
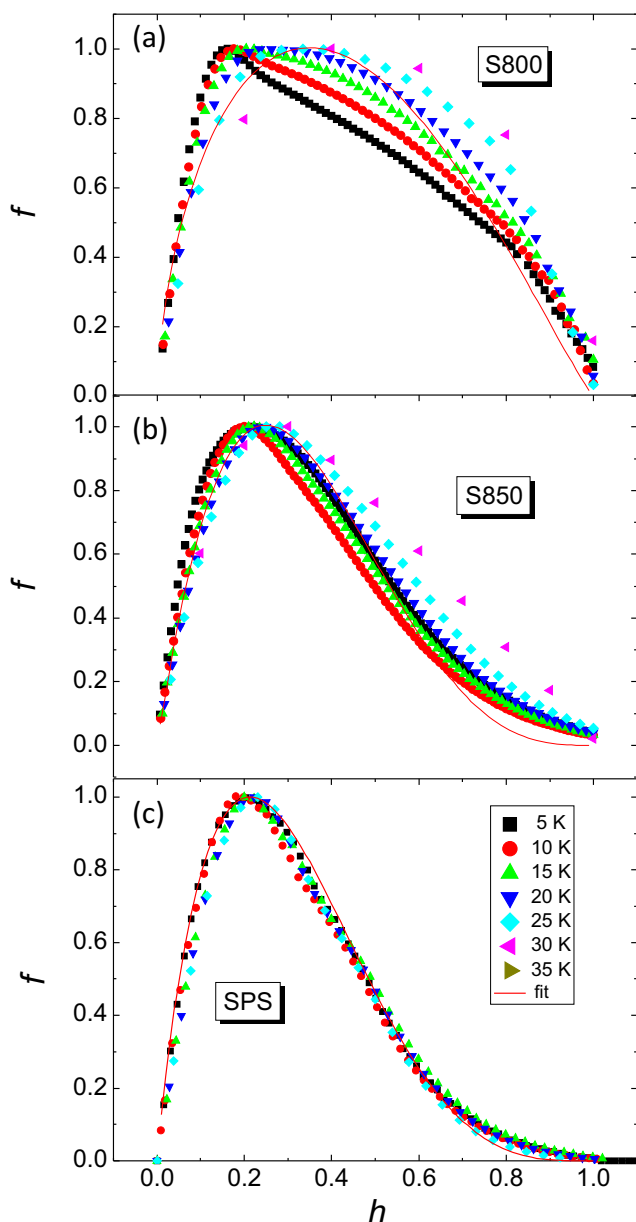
Fig. 1 **a** Pinning force scaling of sample S800. **b** Pinning force scaling of sample S950. **c** Pinning force scaling of sample SPS. The fits to all data according to (1) are indicated by red lines; the obtained fit parameters are listed in Table 1

Figure 2 presents the fit functions obtained for all samples investigated; the corresponding fitting parameters are given in Table 1. Here, we see that the SPS sample shows a clearly different scaling with steep increase at low fields, a peak position, $h_0 = 0.21$, and the typical tail at high fields. All these features are typical for flux pinning provided by the grain boundaries (DH function (3)). The samples S850 and S950 show a less steep increase at low fields, and as consequence, a peak at $h_0 = 0.32/0.33$. This is a strong indication for flux pinning provided by small, non-superconducting defects (DH pinning function (5)). The other samples show an intermediate behavior, but it is important to mention here that the scaling fits of these samples have a much larger deviation as the ones mentioned before. So, one has to admit that these samples do not show a proper pinning force scaling. The main result from the pinning force scaling is that in the sintered samples, flux pinning at GBs is important at lower temperatures, whereas pinning at the small, normal-conducting inclusions is dominating the high field, and high temperature range.

Regarding the values of the scaling parameter p obtained from the fits (see Table 1), we find that all data are ranging in the span of the possible DH values, and the same applies to the q values. Thus, the flux pinning properties of the pure MgB$_2$ samples fit into the scope of the DH approach, which was developed for metallic superconductors. In contrast, on various high-T_c samples, much higher p or q values were found, which reflect a different type of vortex-pin interaction. Furthermore, Table 1 gives the data for the maxima of the pinning forces, $F_{p,max}$, measured via $F_p = j_c \times B$ at a temperature of 10 K. The sample S800 shows slightly higher $F_{p,max}$ as sample S775, and sample S805 has the highest value of all sintered MgB$_2$ samples. The sample S850 exhibits the lowest $F_{p,max}$, and sample S950 reaches

the two scalings is the more pronounced peak in F_p at the low temperatures, the origin of which is discussed in another publication [29]. Note the obvious non-scaling of the data of sample S800, which reveal a clear shift of the peak position and a strengthened high-h part when increasing the temperature. The scalings of samples S850 (b) and S950 are also found to be quite similar to each other. As one can see from the fit functions obtained as shown in Fig. 2 below, the SPS sample (c) reveals in contrast a well-developed scaling behavior.
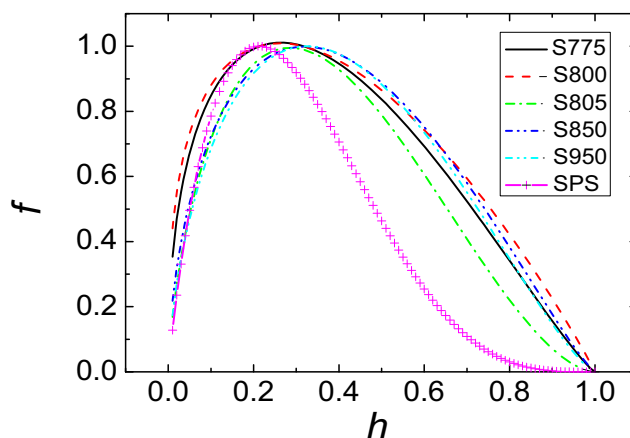

Fig. 2 Summary of all pinning force scalings. Plotted are the fit functions to all data of a sample

again a similar value as the samples S775/S800. In contrast, the SPS sample shows the highest $F_{p,\max}$ measured here.

This non-scaling of the pinning force data may have different reasons. First of all, this non-scaling was observed already by various authors. In Ref. [16], it was speculated that this is due to strongly misoriented MgB_2 grains with the boron plane oriented perpendicular to the applied field. If the field is too strong, these grains would render normal and thus be able to provide more flux pinning according to pinning function (5). As the grains in polycrystalline samples are assumed to be randomly oriented, this is a gradual process according to the crystallographic orientations of the MgB_2 grains. For MgB_2, the anisotropy values γ range in the literature between 1 and 7 [30], so the effect could be a pronounced one. However, our EBSD investigations of the sintered, polycrystalline samples [31] have shown that the MgB_2 grains are not only fully randomly oriented but also have some distinct orientations and practically no fully misoriented grains with a misorientation of 90°. In Ref. [19], we had plotted the temperature dependence of the anisotropy parameter according to Ref. [30] together with the $h_0(T)$ data, and the outcome shows that the anisotropy *reduces* on increasing temperature. Therefore, this explanation for the non-scaling behavior cannot account for the apparent non-scaling.

The strength of the DH scaling analysis is the proper scaling behavior of the pinning forces over a wide temperature range. The so obtained scaling behavior then makes any conclusion about the acting flux pinning mechanism much stronger as if one would analyze the data of only one temperature. However, the present non-scaling of the polycrystalline MgB_2 samples require a different approach to elucidate the ongoing changes with temperature.

As the pinning force scaling of the polycrystalline, sintered MgB_2 samples reveals an apparent non-scaling, we performed the fits of the pinning functions to each measured temperature separately. Although this is, in principle, against the idea of the DH approach, this allows us to get information how the changes of pinning progress when raising the temperature. The results of this procedure are illustrated as the temperature dependence of the peak position, h_0 (Fig. 3) and the temperature dependence of the pinning parameters p and q (Fig. 4a, b) below.

The peak positions, h_0, as function of temperature (Fig. 3) are practically flat for the SPS sample as it is expected from a good scaling at all temperatures. All other samples reveal an increasing h_0 on increase of the temperature. The samples S850 and S950, which show a still acceptable scaling, also exhibit an increase of h_0, but in a limited range only, thus justifying the scaling approach. The other samples reveal a large variation of $h_0(T)$. To compare the temperature-dependent h_0 data with those of the overall
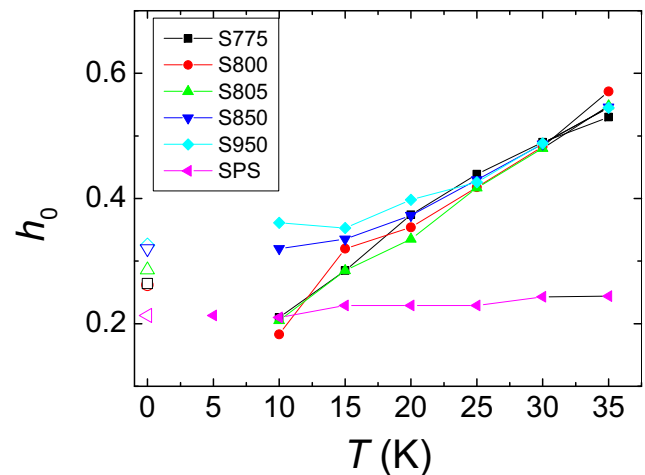

Fig. 3 The peak positions, h_0, as determined from the F_p scalings of each temperature alone. The open symbols plotted at $T = 0$ K give the h_0 values for the common scalings as determined from Fig. 2 for comparison. The lines drawn are guides to the eye

scaling as presented in Fig. 2, we have plotted the resulting peak positions at $T = 0$ using open symbols, but in the same colors. The comparison of these peak positions shows
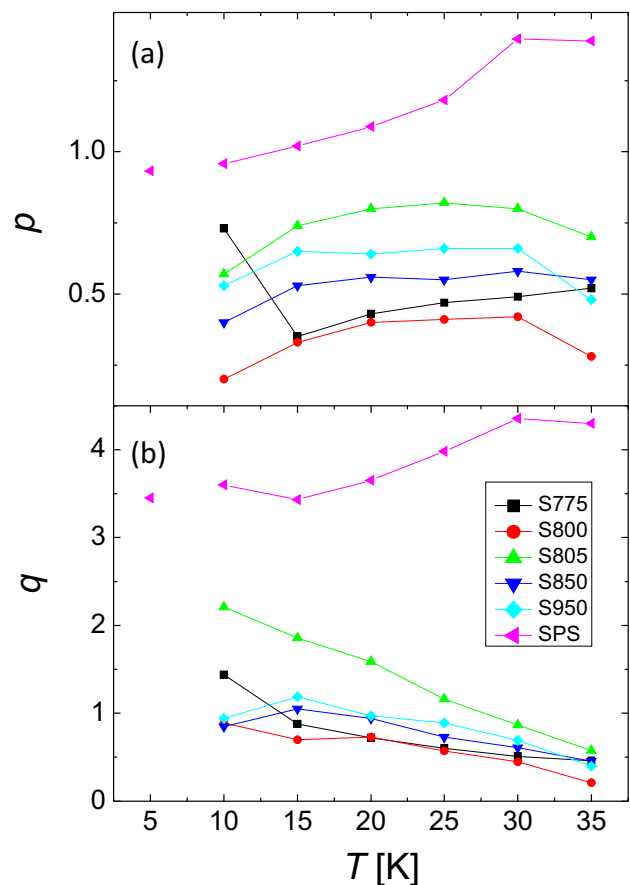

Fig. 4 The variation of the parameters p (**a**) and q (**b**) as a function of temperature using the DH model for each temperature. The lines drawn are guides to the eye

a clear tendency of the overall fits to smooth out the steep increase of h_0 as there are less and less data points at the elevated temperatures.

Figure 4a and b present the temperature dependence of the scaling parameters p and q as obtained from the *individual* fittings to each measured temperature. First of all, one should note that in the original DH scaling, p can take the values of 0, 0.5, 1, 1.5, and 2 (dimensionality and pinning character), and the parameter q can only take the values 1 and 2 (pinning character). Regarding now Fig. 4a, we see that this is not the case for the present data. The data for p range between 0.3 and 1.7, so still in the range of the DH model. The situation is different for the q values, which are around 1 for low T, but then tend clearly down to values around 0.5. The two samples with stronger pinning show high values for q at low T (S805 at ~ 2 and SPS at 3.5), but then the data for sample S805 decrease towards 0.7, whereas the values for the SPS sample even reach $q = 4$. Such high values for q are not uncommon; the pinning force scalings of most high T_c superconductors also exhbit $q > 2$ (see, e.g., [13]).

The pinning force scaling data now suggest another explanation of what is going on in the samples at elevated temperatures. In a previous publication, we discussed the origin of the sharp, narrow peak in the pinning force vs. field diagrams. The reason that this pinning force peak vanishes at higher fields and temperatures was found in the decreasing grain connectivity, which is essential to maintain the current flow through the entire sample. As consequence, this may also take place in our case—at higher magnetic fields, the currents flowing in the samples may circle through smaller entities as the current flow through the entire sample perimeter breaks down after having reached the peak in F_p. The pores being present in the sintered, polycrystalline MgB$_2$ samples also contribute to this effect, forcing the currents on percolative paths.

The most extreme case of this breakdown of the current flow was observed by Dou et al. [32] on compacted and sintered MgB$_2$ samples with grains of a 200-μm size. Here, it was necessary to calculate the current density from the sample perimeter at low fields, and at high fields, the grain size was used instead. In this way, the authors could reconstruct a relatively smooth $j_c(H)$ curve. The appearance of the clear distinction of the two regimes was already seen in the $M(H)$ plots, and the relatively big grain size may be the reason for this observation. The present MgB$_2$ samples have much smaller grains in the 100–500-nm range, so the $M(H)$ loops of all our samples appear fully regular in shape. However, if we presume a change of the current flow radius in the samples, this leads in consequence to a non-scaling behavior of the pinning force data obtained.

Finally, the pinning force scaling as modified by Eisterer [33] is applied to the present data. This approach modifies the DH scaling by using a different scaling field $h = H/H_n$ instead of H_{irr}. Here, H_n denotes the magnetic field, which is reached at 50% above the maximum pinning force. This forces all curves through the point (0.5,1) in the scaling diagram. As a result, the area below $h_n = 1$ is less sensitive to anisotropy and percolation, and the shift of the peak due to this is negligible. If the value of γ changes for example between 2 and 5, the peak shift only causes a deviation of 3% for pinning at grain boundaries.

The fits for this scaling were calculated using the formula as follows:

$$F_p/F_{\mathrm{p,max}} = A \left(\frac{H}{H_n} \right)^p \left(2 - \left(\frac{H}{H_n} \right)^q \right) \quad , \qquad (2)$$

and the resulting temperature dependence of the fit parameters p and q is displayed in Fig. 5a, b.

We have already used the Eisterer scaling to discuss the flux pinning proprties in Ref. [19] and also for carbon-added, polycrystalline MgB$_2$ samples [34]. The advantage of this approach is to take care for the anisotropy and percolation, and thus peak positions smaller than 0.22 can be explained, and the values for h_0 are shifted as compared
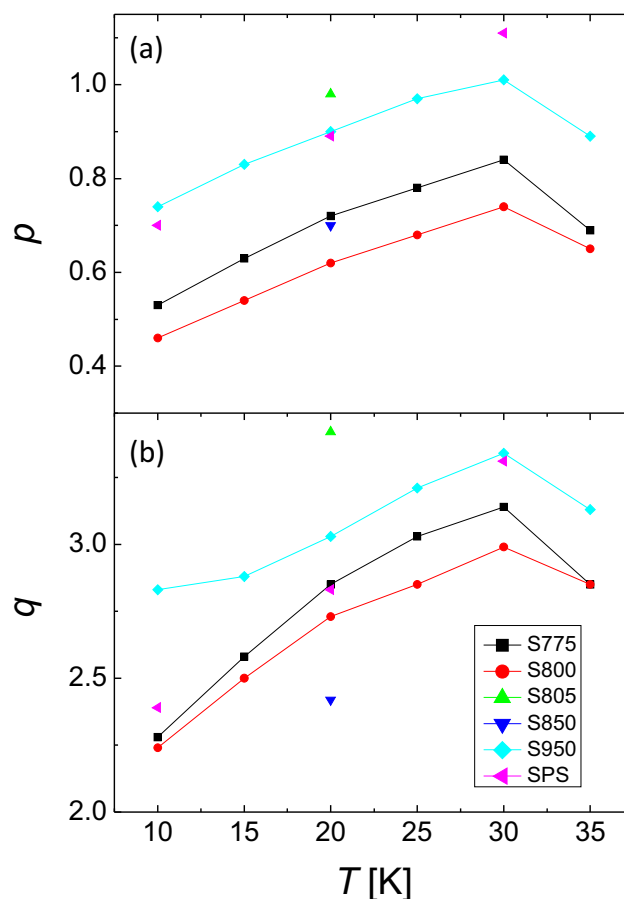

Fig. 5 The variation of the parameters p (**a**) and q (**b**) in the Eisterer scaling. The lines drawn are guides to the eye

to the DH ones. In the present case, the apparent non-scaling of the samples S775, S800, and S805 prevails. The resulting fit parameters p and q exhibit a clear temperature dependence as well. In contrast to the original DH model, the behavior of the parameters p and q shows a common tendency only, which is a drawback of the Eisterer approach. In contrast, nearly common values are found in the DH model when the flux pinning has a common origin. From the data presented here, it is clear that the percolation also changes with increasing temperature, which is another result pointing towards a change of the radius of the current flow. Furthermore, the main result of the DH scaling is also valid when regarding the behavior of the modified scaling of Eisterer.

All the present pinning force scalings demonstrate that the dominating flux pinning in the highly dense SPS sample is provided by the grain boundaries. The scaling works well in the entire temperature range, and the characteristic features of the obtained fitting function are reproduced by all data, even at the highest temperature of $T = 35$ K measured here. On the other side, the scalings of samples S850 and S950 are still acceptable ones, even though the peak positions exhibit a clear upturn on increasing temperature. Here, the pinning is dominantly provided by small, non-superconducting defects, which are highly likely represented by the MgB_4 particles, being created in the samples due to the high reaction temperatures. Both types of scaling (DH and Eisterer) demonstrate the apparent non-scaling of the pinning forces of all other samples studied here. The scalings reveal that for low temperatures, the GBs are the responsible pinning mechanism which changes gradually to pinning at small, normal-conducting inclusions, and even higher peak positions as 0.33 can be obtained, especially at high temperatures. The change of the peak position is further always accompanied by an entire change of the shape of the pinning function. All this leads to the conclusion that there is a change of the current flow radius at elevated temperatures, being due to a gradual decoupling of the MgB_2 grains. This observation has, therefore, important consequences for the development of MgB_2-based superconducting permanent magnets [35–38] with higher trapped fields.

4 Conclusions

To conclude, we performed flux pinning force scalings on a SPS–MgB_2 sample and a series of sintered, polycrystalline MgB_2 samples prepared at various reaction temperatures. The scaling works very well on the SPS sample, indicating a dominant pinning provided by grain boundaries. For the samples sintered at high reaction temperatures, S850 and S950, a still acceptable scaling is obtained which indicates a dominant pinning provided by small, non-superconducting defects. All other samples studied here show an apparent non-scaling, as the peak in f shifts toward higher values on increasing the temperature. Scaling using the Eisterer approach does not provide new insights, but confirms the conclusions drawn from the DH scaling. Thus, the data support the conclusion that at elevated temperature, the MgB_2 grains decouple, and consequently, the current flow in the sample is changed, leading to the apparent non-scaling of the flux pinning forces in some of the samples.

References

1. Eisterer, M.: Magnetic properties, and critical currents of MgB_2. Supercond. Sci Technol. **20**, R47–R74 (2007)
2. Tomsic, M., Rindfleisch, M., Yue, J., McFadden, K., Phillips, J., Sumption, M.D., Bhatia, M., Bohnenstiehl, S., Collings, E.W.: Overview of MgB_2 superconductor applications. Int. J. Appl. Ceram. Technol. **4**, 250–259 (2007)
3. Dou, S.X., Soltanian, S., Horvat, J., Wang, X.L., Zhou, S.H., Ionescu, M., Liu, H.K., Munroe, P., Tomsic, M.: Enhancement of the critical current density and flux pinning of MgB_2 superconductor by nanoparticle doping. Appl. Phys. Lett. **81**, 3419–3421 (2002)
4. Yamamoto, A., Shimoyama, J., Ueda, S., Katsura, Y., Horii, S., Kishio, K.: Improved critical current properties observed in MgB_2 bulks synthesized by low-temperature solid-state reaction. Supercond. Sci. Technol. **18**, 116–121 (2005)
5. Giunchi, G., Ripamonti, G., Cavallin, T., Bassani, E.: The reactive liquid Mg infiltration process to produce large superconducting bulk MgB_2 manufacts. Cryogenics **46**, 237–242 (2006)
6. Mikheenko, P., Martinez, E., Bevan, A., Abell, J.S., MacManus-Driscoll, J.: Grain boundaries and pinning in bulk MgB_2. Supercond. Sci. Technol. **20**, S264–S270 (2007)

7. Martinez, E., Martinez-Lopez, M., Millan, A., Mikheenko, P., Bevan, A., Abell, J.S.: Temperature and magnetic field dependence of the n-values of MgB_2 superconductors. IEEE Trans. Appl. Supercond. **17**, 2738–2741 (2007)

8. Martinez, E., Mikheenko, P., Martinez-Lopez, M., Millan, A., Bevan, A., Abell, J.S.: Flux pinning force in bulk MgB_2 with variable grain size. Phys. Rev. B **75**, 134515 (2007)

9. Cheng, C.H., Sorrell, C.: Defect control at nanoscale and flux pinning enhancement in MgB_2 superconductor. J. Modern Trans. **20**, 65–69 (2012)

10. Naito, T., Sasaki, T., Fujishiro, H.: Trapped magnetic field and vortex pinning properties of MgB_2 superconducting bulk fabricated by a capsule method. Supercond. Sci. Technol. **25**, 095012 (2012)

11. Kramer, E.J.: Scaling laws for flux pinning in hard superconductors. J. Appl. Phys. **44**, 1360–1370 (1973)

12. Dew-Hughes, D.: Flux pinning mechanisms in type-II superconductors. Philos. Mag. **30**, 293–305 (1974)

13. Koblischka, M.R., van Dalen, A.J.J., Higuchi, T., Yoo, S.I., Murakami, M.: Analysis of pinning in $NdBa_2Cu_3O_{7-\delta}$ superconductors. Phys. Rev. B **58**, 2863 (1998)

14. Koblischka, M.R.: Pinning forces and scaling in high-T_c superconductors. Phys. C **282-287**, 2193–2194 (1997)

15. Koblischka, M.R.: Pinning in bulk high-T_c superconductors. Inst. Phys. Conf. Ser. **58**, 1141–1144 (1997)

16. Sandu, V.: Pinning force scaling and its limitation in intermediate and high-temperature superconductors. Mod. Phys. Lett B **26**, 1230007 (2012)

17. Sandu, V., Chee, C.h.J.: On the scaling law of the pinning force in MgB_2 superconducting composites with magnetic nanoinclusions. J. Supercond. Nov. Magn. **26**, 125–131 (2013)

18. Salem, A.F., Ziq, K.A., Bahgat, A.A.: Scaling behavior in aluminium doped MgB_2 superconductor. J. Supercond. Nov. Magn. **26**, 1517–1520 (2013)

19. Koblischka, M.R., Wiederhold, A., Muralidhar, M., Inoue, K., Hauet, T., Douine, B., Berger, K., Murakami, M., Hartmann, U.: Development of MgB_2-based bulk supermagnets. IEEE Trans. Magn. **50**, 9000504 (2014)

20. Badica, P., Aldica, G., Ionescu, A.M., Burdusel, M., Batalu, D.: The influence of different additives on MgB2 superconductor obtained by ex situ spark plasma sintering: pinning force aspects. In: Nishikawa, H., Iwata, N., Endo, T., Takamura, Y., Lee, G.H., Mele, P. (eds.) Correlated functional oxides: nanocomposites and heterostructures, pp. 75–116. Springer, Berlin (2017)

21. Koblischka, M.R., Muralidhar, M.: Pinning force scaling analysis of Fe-based high-T_c superconductors. Int. J. Mod. Phys. B **30**, 1630017 (2016)

22. Noudem, J.G., Aburras, M., Bernstein, P., Chaud, X., Muralidhar, M., Murakami, M.: Development in processing of MgB_2 cryomagnet superconductors. J. Appl. Phys. **116**, 163916 (2014)

23. Noudem, J.G., Dupont, L., Gozzelino, L., Bernstein, P.: Superconducting properties of MgB_2 bulk shaped by spark plasma sintering. Mater. Today-Proc. **3**, 545–549 (2016)

24. Muralidhar, M., Nozaki, K., Kobayashi, H., Zeng, X.L., Koblischka-Veneva, A., Koblischka, M.R., Inoue, K., Murakami, M.: Optimization of sintering conditions in bulk MgB_2 material for improvement of critical current density. J. Alloys Compounds **649**, 833–842 (2015)

25. Koblischka-Veneva, A., Koblischka, M.R., Schmauch, J., Noudem, J., Murakami, M.: Analysis of the microstructure of bulk MgB_2 using TEM, EBSD and t-EBSD. J. Microsc. **274**, 123–131 (2019)

26. Jirsa, M., Rames, M., Koblischka, M.R., Koblischka-Veneva, A., Berger, K., Douine, K.: Relaxation and pinning in spark-plasma sintered MgB_2 superconductor. Supercond. Sci. Technol. **29**, 025006 (2016)

27. Berger, K., Koblischka, M.R., Douine, B., Noudem, J., Bernstein, P., Hauet, T., Leveque, J.: High magnetic field generated by bulk MgB_2 prepared by spark plasma sintering. IEEE Trans. Appl. Supercond. **29**, 6801005 (2016)

28. Wiesinger, H.P., Sauerzopf, F.M., Weber, H.W.: On the calculation of J_c from magnetization measurements on superconductors. Phys. C **203**, 121–128 (1992)

29. Koblischka, M.R., Wiederhold, A., Koblischka-Veneva, A., Chang, C., Berger, K., Nouailhetas, Q., Douine, B., Murakami, M.: Origin of the sharp, low-field peak in MgB_2 superconductors. submitted for publication. AIP Adv. **10**, 015035 (2020)

30. Shi, Z.X., Tokunaga, M., Tamegai, T., Takano, Y., Togano, K., Kito, H., Ihara, H.: Out-of-plane and in-plane anisotropy of upper critical field in MgB_2. Phys. Rev. B **68**, 104513 (2003)

31. Koblischka-Veneva, A., Koblischka, M.R., Schmauch, J., Inoue, K., Muralidhar, M., Berger, K., Noudem, J.: EBSD analysis of MgB_2 bulk superconductors. Supercond. Sci. Technol. **29**, 044007 (2016)

32. Dou, S.X., Wang, X.L., Horvat, J., Milliken, D., Li, A.H., Konstantinov, K., Collings, E.W., Sumption, M.D., Liu, H.K.: Flux jumping and a bulk-to-granular transition in the magnetization of a compacted and sintered MgB_2 superconductor. Phys. C **361**, 79–83 (2001)

33. Eisterer, M.: Calculation of the volume pinning force in MgB_2 superconductors. Phys. Rev. B **77**, 144524 (2008)

34. Koblischka, M.R., Koblischka-Veneva, A., Muralidhar, M., Murakami, M.: Magnetic characterization of bulk C-added MgB_2. IEEE Trans. Appl. Supercond. **29**, 6800104 (2019)

35. Fuchs, G., Häßler, W., Nenkov, K., Scheiter, J., Perner, O., Handstein, A., Kanai, T., Schultz, L., Holzapfel, B.: High trapped fields in bulk MgB_2 prepared by hot-pressing of ball-milled precursor powder. Supercond. Sci. Technol. **26**, 122002 (2012)

36. Durrell, J.H., Dancer, C.E.J., Dennis, A., Shi, Y., Xu, Z., Campbell, A.M., Babu, N.H., Todd, R.I., Grovenor, C.R.M., Cardwell, D.A.: A trapped field of >3 T in bulk MgB_2 fabricated by uniaxial hot pressing. Supercond. Sci. Technol. **25**, 112002 (2012)

37. Berger, K., Koblischka, M.R., Douine, B., Noudem, J., Bernstein, P., Hauet, T., Lévêque, J.: High magnetic field generated by bulk MgB_2 prepared by spark plasma sintering. IEEE Trans. Appl. Supercond. **26**, 6801005 (2016)

38. Miyazaki, T., Fukui, S., Ogawa, J., Sato, T., Oka, T., Scheiter, J., Häßler, W., Kulawansha, E., Yuanding, Z., Yokoyama, K.: Pulse-field magnetization for disc-shaped MgB_2 bulk magnets. IEEE Trans. Appl. Supercond. **27**, 6800504 (2017)